Effect of atomic disorder on electronic, magnetic and electron-transport properties of Ti_2MnAl

Pavel V. Lukashev[1#], Zachary Lehmann[2], Lukas Stuelke[1], Randall Filippone[3], Bishnu Dahal[2], Shah Valloppilly[4], Jace Waybright[5], Arjun K. Pathak[3], Yung Huh[2], Paul M. Shand[1], and Parashu Kharel[2*]

[1]*Department of Physics, University of Northern Iowa, Cedar Falls, IA 50614, USA*
[2]*Department of Physics, South Dakota State University, Brookings, SD 57007, USA*
[3]*Department of Physics, SUNY, Buffalo State, Buffalo, NY, 14222, USA*
[4]*Nebraska Center for Materials and Nanoscience, University of Nebraska, Lincoln, NE 68588, USA*
[5]*Department of Astrophysical Sciences, Princeton University, Princeton, NJ 08540, USA*

pavel.lukashev@uni.edu
* *parashu.kharel@sdstate.edu*

Abstract

We report the combined computational and experimental study on the effect of atomic disorder on electronic, magnetic, and electron-transport properties of Ti_2MnAl Heusler alloy. Ti_2MnAl is predicted to exhibit spin-gapless semiconducting behavior in the inverted cubic crystal structure, while the regular cubic structure is essentially non-spin-polarized and non-magnetic. Here, we analyze three types of atomic disorder, namely, A2, B2, and $D0_3$, which are commonly observed in Heusler alloys. Our first-principles calculations indicate that all three types of disorder have a relatively small effect on a non-spin-polarized nature of Ti_2MnAl in the regular cubic crystal (prototype Cu_2MnAl) structure. At the same time, the inverted cubic phase (prototype Hg_2TiCu) retains a significant degree of spin-polarization in A2 and B2 disordered structures. In particular, A2 and B2 types of disorder of the inverted cubic phase result in a spin-polarization of about 50% and 74%, respectively. The $D0_3$ disordered inverted phase has a significantly smaller spin-polarization of less than 10%. All considered structures align ferrimagnetically, except the B2-disordered and non-disordered regular cubic phases, which are non-magnetic. Our experimental results are consistent with the predicted properties of Ti_2MnAl with partial A2 and B2 disorder types. While atomic disorder in a considered system should be minimized or avoided for practical implementations, its type may play a decisive role for potential applications in spin-based electronics.

I. Introduction

Over the last few decades, one of the most actively developing branches of materials science has been spintronics – an emerging technology utilizing a spin degree of freedom in electronic devices. Materials with a high degree of spin polarization are in demand in this field for device applications. In particular, room-temperature half-metals (HM) may be considered as ideal candidates, as they exhibit perfect spin-polarization, i.e., they behave as an insulator for one spin channel and a conductor for the other spin channel.[1,2,3,4,5,6,7,8,9,10] Recently, another class of materials, spin-gapless semiconductors, has attracted significant attention due to potential practical applications in spintronics.[11,12,13,14,15] These materials exhibit zero band gap in one spin channel and a finite bandgap in the opposite channel. Spin-gapless semiconductors (SGS) may potentially exhibit several remarkable properties such as perfect spin polarization (100%) of both the electrons and holes, high carrier mobilities, ability to switch between spin-polarized *n*- and *p*-type conduction, etc.[16]

The attractive features of HM and SGS materials reported in the literature, in particular their 100% spin-polarization, are often based on theoretical predictions that consider somewhat idealized systems without any lattice imperfections or atomic disorder. The latter, however, can rarely be eliminated in the realistic experimental setup, and typically results in reduced spin-polarizations, as compared with an idealized system.[17] In X_2YZ Heusler alloys, two commonly encountered types of disorder are A2 and B2, which are caused by X-Z and Y-Z mixings, respectively. Another type of disorder observed in X_2YZ full Heusler alloys is $D0_3$, which is caused by X-Y mixing.[18] Here, we present a combined experimental and computational study of these three types of atomic disorder in Ti_2MnAl. We present a theoretical investigation of the effect of A2, B2, and $D0_3$ disorder on the electronic band structure and magnetic properties of both regular cubic and inverted cubic Ti_2MnAl. In addition, we investigate the structural, magnetic, and electron-transport properties of the bulk Ti_2MnAl alloy.

The interest in Ti_2MnAl stems from the predicted spin-gapless semiconducting properties with compensated ferrimagnetic order[19,20] and a topological state[21] in its inverted cubic crystal structure. In our recent work, we showed that Ti_2MnAl may exhibit spin-gapless semiconductivity in the inverted cubic Heusler crystal structure, while the regular Heusler crystal structure is nearly non-spin-polarized.[22] Experimental work on structural and magnetic properties of A2 disordered

bulk Ti_2MnAl has been reported, which is consistent with the predicted properties of regular cubic Ti_2MnAl.[23] Another report on thin-film Ti_2MnAl claims that the observed magnetic and transport properties are similar to that of a spin-gapless semiconductor.[24] Our experimental results on disordered Ti_2MnAl are slightly different from both of these reports, indicating that the properties of Ti_2MnAl are sensitive to both elemental composition as well as the type and degree of disorder.

II. Methods

II-1. Computational methods

We perform density functional calculations on bulk Ti_2MnAl full Heusler alloy, using the projector augmented-wave method (PAW),[25] implemented in the Vienna *ab initio* simulation package (VASP)[26] within the generalized-gradient approximation (GGA).[27] The integration method[28] with a 0.05 eV width of smearing is used. The cut-off energy of the plane-waves is set to 500 eV. Structural optimization is performed with the energy convergence criterion of 10^{-2} meV, which results in the Hellmann-Feynman forces being less than 0.005 eV/Å. The total energy and electronic structure calculations are performed with a stricter convergence criterion of 10^{-3} meV. The Brillouin zone integration is performed with a *k*-point mesh of 12 × 12 × 12. Some of the results and figures (such as the crystal structure visualization) are obtained using the MedeA® software environment.[29] Most of the calculations were performed using Extreme Science and Engineering Discovery Environment (XSEDE) resources located at the Pittsburgh Supercomputing Center (PSC),[30] and the resources of the Center for Functional Nanomaterials (CFN) at Brookhaven National Laboratory (BNL).

II-2. Experimental methods

Ti_2MnAl ingots were prepared using arc melting and high-vacuum annealing. First, pieces of highly pure (99.99%) Ti, Mn, and Al with proper weight ratio were cut from corresponding commercially available pellets and melted on a water-cooled Cu hearth of an arc furnace in an argon environment. The subsequent annealing of each sample was performed in a tubular vacuum furnace ($\sim 10^{-7}$ torr) at 500°C for 48 hours to further homogenize the samples. The crystal structures of the samples were analyzed using a Rigaku MiniFlex600 x-ray diffractometer with a

Cu-Kα source (λ = 1.54 Å). The elemental compositions of the annealed samples were confirmed using energy-dispersive x-ray spectroscopy (EDS). The elemental composition as determined by EDS is $Ti_{2.07}Mn_{0.95}Al_{0.98}$ which is very close to the nominal composition. A Quantum Design VersaLab magnetometer and a Dynacool PPMS system were used to investigate the magnetic and electron transport properties.

III. Results and discussion

III-1. Computational results

In our recent work, we reported that a full Heusler compound Ti_2MnAl is likely to crystallize in the regular cubic Heusler structure (prototype Cu_2MnAl), with an inverted cubic Heusler polymorph (prototype $CuHg_2Ti$) with slightly higher energy and an SGS band structure with zero net magnetic moment, which is a result of fully compensated ferrimagnetic alignment.[22] These structures are illustrated in Fig. 1, and are referred as "regular" and "inverted" phases in the rest of the paper. In what follows, we consider three types of atomic disorder in these two structures: A2-type disorder, where Ti and Al atoms are swapped; B2-type disorder, where Mn and Al atoms are swapped; and $D0_3$-type disorder, where Ti and Mn atoms are swapped. For all three types of disorder, we swapped one atom of a given element with one atom of another element, with all calculations performed in a 16-atom cell, i.e. $Ti_8Mn_4Al_4$. For each of the considered cases, we determined the minimum energy configuration before proceeding to the electronic and magnetic structure calculations. The atomic positions and calculated magnetic moments of all considered structures are presented in the Appendix.

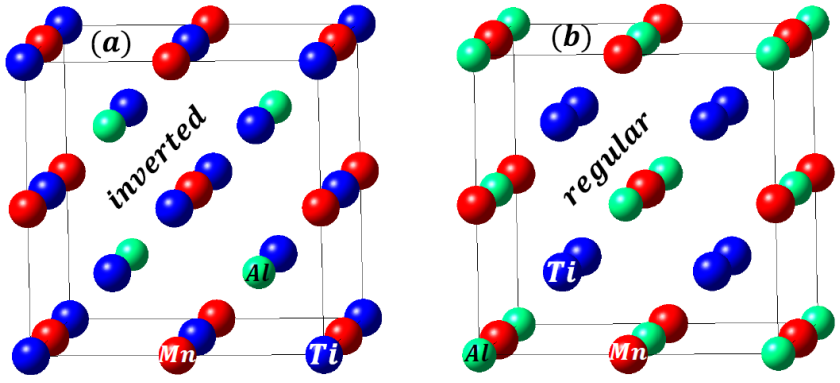

Figure 1: Ti_2MnAl in inverted (a) and regular (b) crystal structures. Atoms are labeled on the figure (blue – Ti, red – Mn, green – Al).

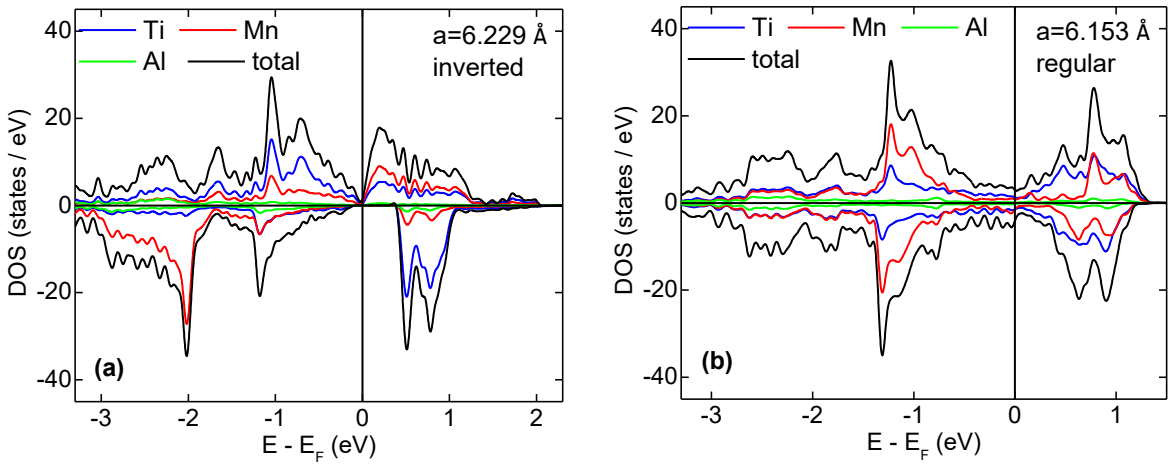

Figure 2: Calculated DOS of Ti_2MnAl in inverted (a) and regular (b) crystal structures. Elemental contributions are color-coded as indicated in the figure.

Fig. 2 shows the calculated density of states (DOS) of the inverted (a) and regular (b) cubic phases of Ti_2MnAl, with the equilibrium lattice parameters as indicated in the figure. As noted above, the inverted phase exhibits a spin-gapless semiconducting electronic structure, while the regular phase is essentially non-spin-polarized and non-magnetic, consistent with recent report by Özdoğan and Galanakis.[31] In addition, the magnetic alignment of the inverted phase is fully compensated ferrimagnetic, with zero net magnetization, which makes it attractive for practical implementations, where stray magnetic fields are to be avoided.

Figures 3, 4, and 5 show calculated DOS of the inverted (a) and regular (b) phases of B2-disordered, A2-disordered, and $D0_3$-disordered Ti_2MnAl, correspondingly (equilibrium lattice parameters are shown in the figure). As one can see from Figures 3 (b), 4 (b), and 5(b), all three types of atomic disorder have a relatively small effect on the nearly non-spin-polarized nature of the regular cubic phase. At the same time, while all three types of disorder destroy the spin-gapless semiconducting nature of the inverted phase (see Figures 3 (a), 4 (a), and 5 (a)), it still retains a significantly high degree of spin polarization in A2- and B2-disordered structures (about 50% and 74%, correspondingly). The $D0_3$ type of disorder has a significantly more detrimental impact on a spin-polarization of the inverted phase, reducing it to under 10%. Table 1 shows calculated magnetic alignments and spin-polarization values (defined as $P = \frac{N_\uparrow(E_F) - N_\downarrow(E_F)}{N_\uparrow(E_F) + N_\downarrow(E_F)}$, where $N_{\uparrow\downarrow}(E_F)$ is the spin-dependent density of states at the Fermi level, E_F)[32] for all considered structures.

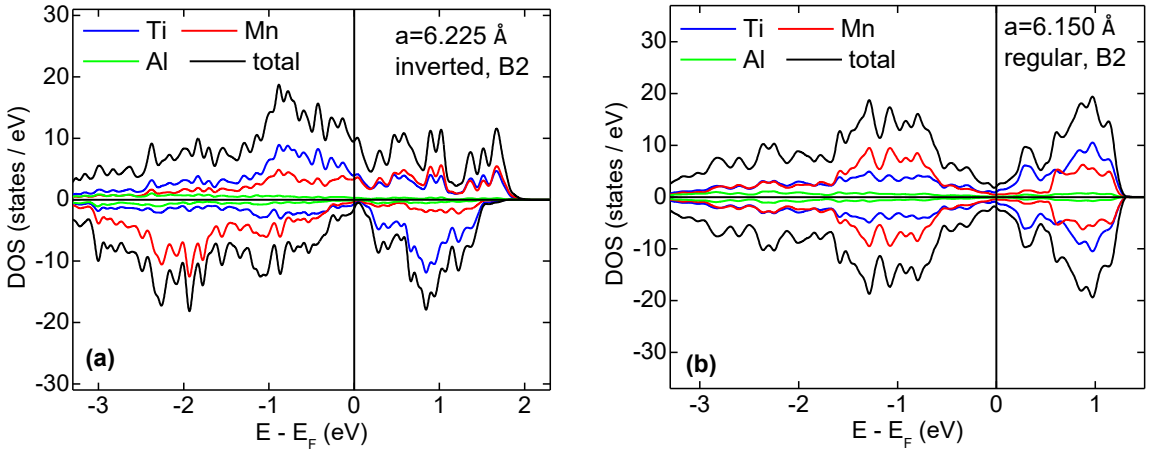

Figure 3: Calculated DOS of B2-disordered Ti_2MnAl in inverted (a) and regular (b) crystal structures. Elemental contributions are color-coded as indicated in the figure.

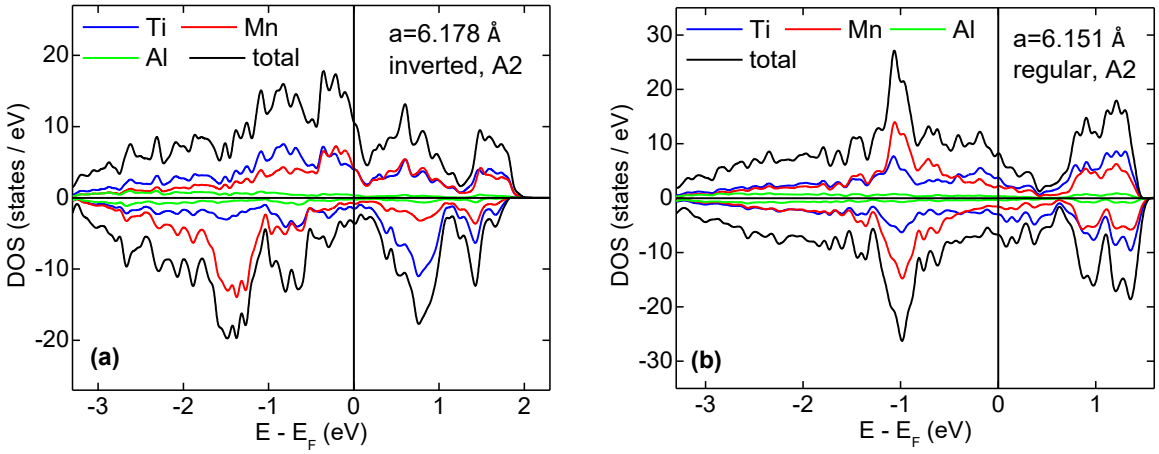

Figure 4: Calculated DOS of A2-disordered Ti_2MnAl in inverted (a) and regular (b) crystal structures. Elemental contributions are color-coded as indicated in the figure.

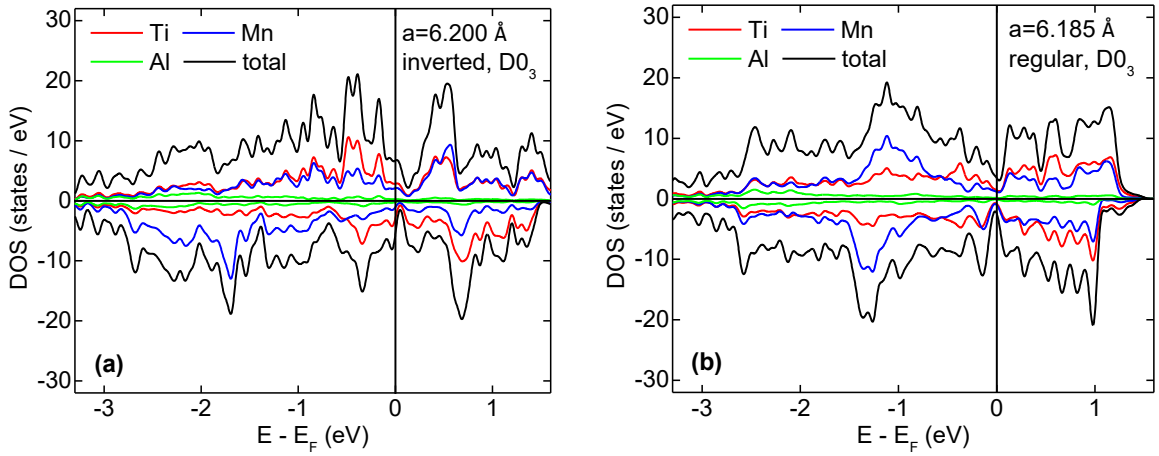

Figure 5: Calculated DOS of $D0_3$-disordered Ti_2MnAl in inverted (a) and regular (b) crystal structures. Elemental contributions are color-coded as indicated in the figure.

Figure 6 (a) shows the calculated energies of all eight considered structures. As one can see, the regular cubic phase with B2 disorder is energetically favorable. This is also the only disordered phase, which, according to our calculations, is non-magnetic. The second energetically favorable phase is regular cubic without the atomic disorder, followed by the ordered inverted phases. The energy difference between these phases is relatively small, thus indicating a possible structural transition, e.g., under mechanical strain.[22] The other considered phases are also energetically close. Therefore, in the experiment, any of these phases can be potentially stabilized depending on the method of materials synthesis and slight variation in chemical composition.

	Crystal structure	Magnetic alignment	Spin-polarization (%)
1	Inverted, no disorder	ferrimagnetic	99.9%
2	Inverted, A2-disorder	ferrimagnetic	49.5%
3	Inverted, B2-disorder	ferrimagnetic	73.8%
4	Regular, no disorder	non-magnetic	-15.4% *(see caption)*
5	Regular, A2-disorder	ferrimagnetic	10.1%
6	Regular, B2-disorder	non-magnetic	-0.1%
7	Inverted, $D0_3$-disorder	ferrimagnetic	8.7%
8	Regular, $D0_3$-disorder	ferrimagnetic	16.8%

Table 1: Calculated magnetic alignment and spin-polarization of Ti_2MnAl in all eight considered crystal structures. *The reported non-zero value of spin polarization of regular non-disordered structure is probably a computational artifact. The calculated magnetic moments per atom of this structure are very small (see Appendix), which makes this structure essentially non-magnetic.*

Figure 6 (b) shows calculated lattice constants (black line and squares) and magnetic moment per 16-atom cell (blue lines and circles) of Ti_2MnAl in all eight considered crystal structures (the numbering of the structures is consistent with the one shown in Fig. 6 (a); see caption of the figure). One important result here is that both ordered and B2-disordered inverted cubic phases exhibit perfect or nearly perfect fully compensated ferrimagnetic alignment, which may be appealing for practical device applications, where internal magnetic fields are undesirable.

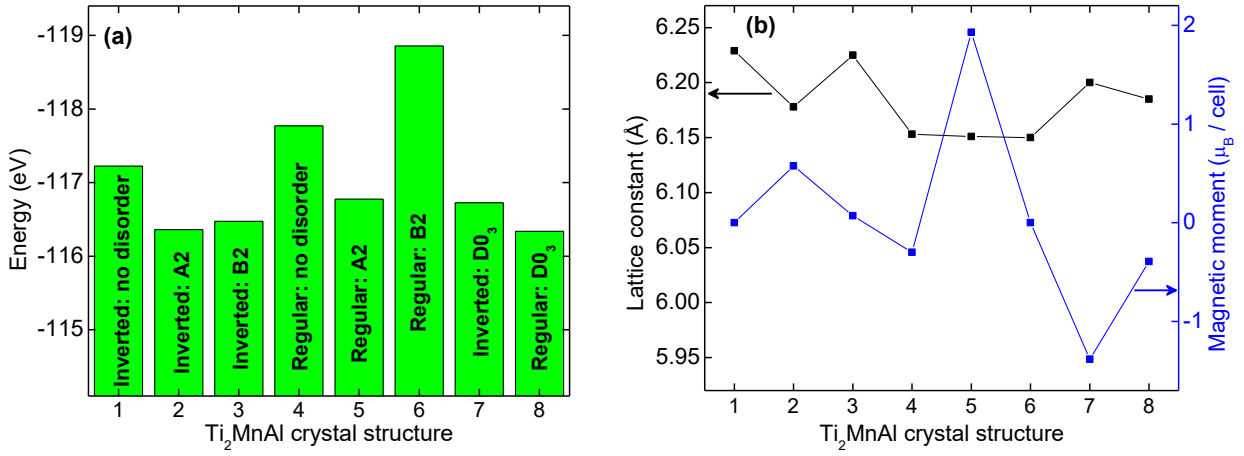

Figure 6: (a) Calculated energies of Ti_2MnAl in all eight considered crystal structures, as indicated in the figure. (b) Calculated lattice constants (black line and squares) and magnetic moment per 16-atom cell (blue lines and circles) of Ti_2MnAl in all eight considered crystal structures (the numbering of the structures is consistent with the one shown in Fig. 6 (a), i.e. "1" corresponds to inverted phase with no disorder, "2" corresponds to inverted phase with A2 disorder, etc.).

III-2. Experimental results

The room-temperature XRD patterns of the powder samples prepared from as-prepared and annealed Ti_2MnAl ingots are shown in Figs. 7(a) and 7(b), respectively. As shown in the figures, the most intense peaks in the XRD patterns are indexed with the standard pattern for cubic Ti_2MnAl. In order to find whether the experimental patterns belong to the regular cubic or inverted cubic phases of Ti_2MnAl and to understand the nature and amount of disorder, we performed Rietveld analyses of the XRD patterns. For the as-prepared sample, the characteristic Heusler (111) and (002) peaks are absent; hence, it can be assumed that the structure would have stabilized with a highly disordered A2 type structure. Full profile analysis also suggests the A2-type structure fits the experimental data best. The annealed sample shows the presence of a significant (002) peak, suggesting a higher degree of ordering; however, the absence of the (111) peak is an indication that the fully ordered regular or inverse cubic Heusler structure may not have been formed. Nevertheless, some site disorder and the scattering factor of the elements occupying those sites could influence the diffraction intensities of these characteristic peaks. Therefore, we analyzed the XRD pattern of the annealed sample by the Rietveld method incorporating various types of site disorder, namely, A2, B2, and $D0_3$. The best fit was obtained for a B2-disordered regular Heusler

structure as depicted in the inset of Fig 7(b). In this model, Ti atoms occupy the 8c sites and Mn and Al atoms are evenly distributed at the 4a and 4b sites. The lattice parameters obtained from this analysis are 6.206 Å and 6.212 Å for as-prepared and annealed Ti_2MnAl, respectively. Therefore, after annealing, the crystalline order improved and the samples show partial ordering with B2-type disorder present between Mn and Al. This result is consistent with the theoretical prediction that the most stable phase of Ti_2MnAl is the B2 disordered regular cubic structure.

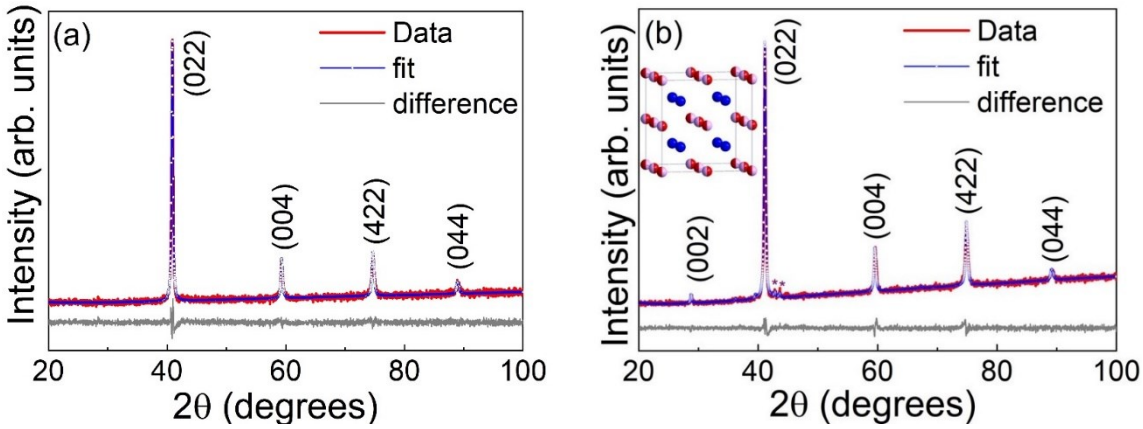

Figure 7: Room temperature x-ray diffraction patterns of (a) as-prepared and (b) annealed Ti_2MnAl samples. Experimental data, Rietveld simulations, and the difference curves are shown in both figures. As mentioned in the text, a fully disordered A2-type structure was used for the as-prepared sample, whereas a partially disordered B2-type (as shown in the inset) was found to be appropriate for the annealed sample. The peaks indicated by a star are from unknown impurity.

The magnetization as a function of magnetic field *M(H)* measured at 5 K for the as-prepared and annealed Ti_2MnAl bulk samples are shown in Figs. 8(a) and 8(b), respectively. The low temperature *M(H)* curves for both samples are not saturated at 80 kOe field and the *M(H)* curve of the annealed sample is almost linear. There are no noticeable hysteresis in the *M(H)* curves of both samples. However, the *M(H)* curve of the as-prepared sample is not completely linear as expected in paramagnetic or antiferromagnetic materials. The non-zero remance in the as-prepared sample is attributed to the A2 disorder in the sample. Further, the low-temperature magnetizations at 80 kOe for both the samples are very small, namely, 0.36 emu/g (0.013 μ_B / f.u) and 0.23 emu/g (0.008 μ_B/f.u.) for the as prepared and annealed samples, respectively. Although the low temperature magnetization for the as-prepared sample is larger than that of the annealed sample as expected by theory, the magnitudes of the magnetizations are slightly different from expected values, which can be attributed to incomplete A2 and B2 disorders in the samples.

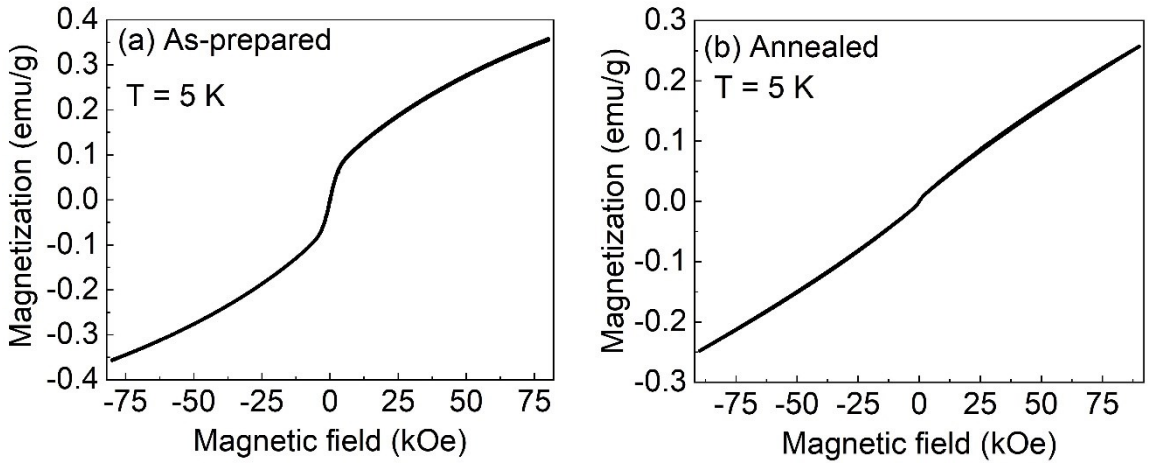

Figure 8: Isothermal magnetization curves *M(H)* measured at 5 K on (a) as prepared and (b) annealed Ti_2MnAl samples.

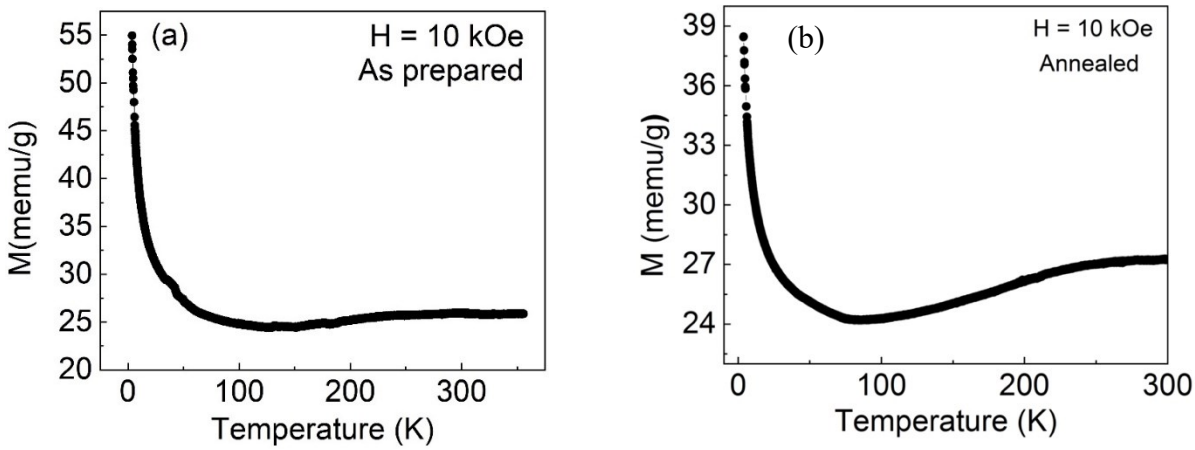

Figure 9: Thermomagnetic curves *M(T)* measured at 10 kOe on (a) as prepared and (b) annealed Ti_2MnAl samples.

Figures 9(a) and 9(b) respectively show thermomagnetic curves *M(T)* of as-prepared and annealed Ti_2MnAl samples measured in a constant magnetic field of 10 kOe. As shown in the figures, the magnetizations of both the samples first decrease as temperature increases from 4 K, reach corresponding minima, and increase with further increase in temperature. The magnetization minimum in the *M(T)* curve of the as-prepared sample is around 130 K. This behavior is more pronounced in the annealed sample. These magnetization behaviors are slightly different from the

one reported in the recent work by Goraus and Czerniewski for A2 disordered regular cubic bulk Ti_2MnAl, where they have shown a pure paramagnetic behavior.[23] The behavior of the *M(T)* curves is likely due to the variation of the anisotropy constants with temperature. Generally, the strength of the anisotropy increases as the temperature decreases; thus, the magnetization well below the Curie temperature tends to decrease in relatively small fields. However, in many cases, the variation of the anisotropy constants with temperature is non-monotonic, which could lead to the observed minima. The sharp upturn at very low temperatures is attributable to uncompensated spins in the spatially inhomogeneous ferrimagnetic system resulting from partial B2 or A2 disorder.

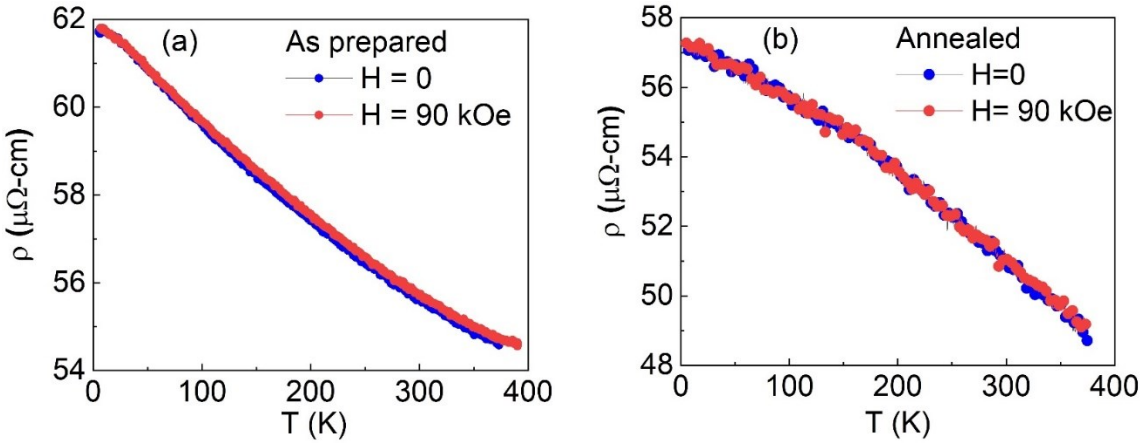

Figure 10: Temperature dependence of resistivity measured at 0 and 90 kOe on (a) as prepared and (b) annealed Ti_2MnAl samples.

The resistivity as a function of temperature $\rho(T)$ measured at $H = 0$ and 90 kOe for the as-prepared and annealed Ti_2MnAl bulk samples are shown in Figs. 10(a) and 10(b), respectively. The electrical resistivities were measured for both as-prepared and annealed samples at H = 0 and 90 kOe using a standard four-probe technique. The sample was cut into a small rectangular bar with dimensions 4 mm × 2.5 mm × 1.5 mm. As shown in Fig. 10, both samples show a very small negative temperature coefficient of resistivity (TCR) and there is no discernible effect of the magnetic field on the resistivity. The values of TCR measured in our samples (-1.9 $\times 10^{-8}\,\Omega cmK^{-1}$ for the as-prepared sample, and $-2.3 \times 10^{-8}\,\Omega cmK^{-1}$ for the annealed

sample) are very close to the one observed in arc-melted Mn_2CoAl.[33] The resistivity of the as-prepared sample smoothly decreases with increasing temperature similar to that of a classical semiconductor, whereas that of the annealed sample shows a small slope change near 120 K and then decreases almost linearly with a further increase in temperature. This temperature is slightly above the magnetization minimum observed in its *M(T)* curve. Further, the low-temperature resistivity of the annealed sample is slightly smaller (57 $\mu\Omega cm$) than that (62 $\mu\Omega cm$) of the as-prepared sample. This may be due to different types of disorder present in these two samples. The observed $\rho(T)$ behavior of the annealed sample is exceptional and very different from that of the classical semiconductors. The negative temperature coefficient of resistivity has also been reported in semiconducting materials and highly disordered materials. The negative TCR in transition metal alloys has been attributed to the strong impurity scattering.[34] However, similar linear behavior of resistivity with a slope change at low temperature has been reported in predicted spin-gapless semiconducting materials including Mn_2CoAl, CoCrFeAl, and Ti_2MnAl films.[35,36,37] The slight slope change in $\rho(T)$ curve of spin-gapless semiconductors is attributed to its special type of band structure. Based on our calculations, the spin-gapless semiconducting behavior is not expected in B2 disordered regular cubic structure of Ti_2MnAl. Yet, the observed resistivity of our annealed sample is unique and may be attributed to atomic disorder.

IV. Conclusions

In conclusion, we analyzed the effect of three types of atomic disorder, namely, A2, B2, and $D0_3$ on electronic, magnetic, and electron transport properties of Ti_2MnAl, a potential spin-gapless semiconductor. Based on our calculations, all three types of disorder have a relatively small effect on the non-spin-polarized character of Ti_2MnAl in the regular crystal structure. However, the inverted cubic phase retains a significantly high degree of spin-polarization in A2 and B2 disordered structures. In particular, A2 type disorder of the inverted phase results in a spin-polarization of about 50%, B2 type disorder of the same phase exhibits around 74% spin-polarization. The magnetic alignments in all the considered structures are ferrimagnetic, except in the B2-disordered regular phase, which is non-magnetic. The experimental magnetic and electron transport properties are similar to those predicted for the regular cubic phase of this material with partial A2 and B2 type disorder, respectively. Since thin films are desired for device applications,

our results may stimulate interest in high-quality thin-film synthesis, potentially leading to an implementation of this material in spin-transport-based devices.

Appendix

Tables below present calculated magnetic moment per atom and atomic coordinates of all eight considered structures, for 16-atom supercells.

		Inverted				Regular			
		ideal	A2	B2	$D0_3$	ideal	A2	B2	$D0_3$
Ti-1	position	$(0;0;0)$	$\left(\frac{3}{4};\frac{1}{4};\frac{1}{4}\right)$	$(0;0;0)$	$\left(\frac{1}{2};\frac{1}{2};\frac{1}{2}\right)$	$(0;0;0)$	$\left(\frac{3}{4};\frac{1}{4};\frac{1}{4}\right)$	$(0;0;0)$	$\left(\frac{1}{4};\frac{3}{4};\frac{3}{4}\right)$
		$\left(\frac{1}{2};\frac{1}{2};0\right)$	$\left(\frac{1}{2};\frac{1}{2};0\right)$	$\left(\frac{1}{2};\frac{1}{2};0\right)$	$\left(\frac{1}{2};\frac{1}{2};0\right)$	$\left(\frac{1}{2};\frac{1}{2};0\right)$	$\left(\frac{1}{2};\frac{1}{2};0\right)$	$\left(\frac{1}{2};\frac{1}{2};0\right)$	$\left(\frac{1}{2};\frac{1}{2};0\right)$
		$\left(\frac{1}{2};0;\frac{1}{2}\right)$	$\left(\frac{1}{2};0;\frac{1}{2}\right)$	$\left(\frac{1}{2};0;\frac{1}{2}\right)$	$\left(\frac{1}{2};0;\frac{1}{2}\right)$	$\left(\frac{1}{2};0;\frac{1}{2}\right)$	$\left(\frac{1}{2};0;\frac{1}{2}\right)$	$\left(\frac{1}{2};0;\frac{1}{2}\right)$	$\left(\frac{1}{2};0;\frac{1}{2}\right)$
		$\left(0;\frac{1}{2};\frac{1}{2}\right)$	$\left(0;\frac{1}{2};\frac{1}{2}\right)$	$\left(0;\frac{1}{2};\frac{1}{2}\right)$	$\left(0;\frac{1}{2};\frac{1}{2}\right)$	$\left(0;\frac{1}{2};\frac{1}{2}\right)$	$\left(0;\frac{1}{2};\frac{1}{2}\right)$	$\left(0;\frac{1}{2};\frac{1}{2}\right)$	$\left(0;\frac{1}{2};\frac{1}{2}\right)$
	mag. mom.	1.082	0.505	0.945	-0.616	0.062	0.760	0.000	-0.002
		1.082	0.819	0.912	0.647	0.062	0.128	0.000	0.107
		1.082	0.819	0.912	0.647	0.062	0.128	0.000	0.107
		1.082	0.819	0.912	0.647	0.062	0.128	0.000	0.107
Ti-2	position	$\left(\frac{1}{4};\frac{1}{4};\frac{1}{4}\right)$	$\left(\frac{1}{4};\frac{1}{4};\frac{1}{4}\right)$	$\left(\frac{1}{4};\frac{1}{4};\frac{1}{4}\right)$	$\left(\frac{1}{4};\frac{1}{4};\frac{1}{4}\right)$	$\left(\frac{1}{2};\frac{1}{2};\frac{1}{2}\right)$	$\left(\frac{1}{2};\frac{1}{2};\frac{1}{2}\right)$	$\left(\frac{1}{2};\frac{1}{2};\frac{1}{2}\right)$	$\left(\frac{1}{2};\frac{1}{2};\frac{1}{2}\right)$
		$\left(\frac{3}{4};\frac{3}{4};\frac{1}{4}\right)$	$\left(\frac{3}{4};\frac{3}{4};\frac{1}{4}\right)$	$\left(\frac{3}{4};\frac{3}{4};\frac{1}{4}\right)$	$\left(\frac{3}{4};\frac{3}{4};\frac{1}{4}\right)$	$\left(\frac{1}{2};0;0\right)$	$\left(\frac{1}{2};0;0\right)$	$\left(\frac{1}{2};0;0\right)$	$\left(\frac{1}{2};0;0\right)$
		$\left(\frac{3}{4};\frac{1}{4};\frac{3}{4}\right)$	$\left(\frac{3}{4};\frac{1}{4};\frac{3}{4}\right)$	$\left(\frac{3}{4};\frac{1}{4};\frac{3}{4}\right)$	$\left(\frac{3}{4};\frac{1}{4};\frac{3}{4}\right)$	$\left(0;\frac{1}{2};0\right)$	$\left(0;\frac{1}{2};0\right)$	$\left(0;\frac{1}{2};0\right)$	$\left(0;\frac{1}{2};0\right)$
		$\left(\frac{1}{4};\frac{3}{4};\frac{3}{4}\right)$	$\left(\frac{1}{4};\frac{3}{4};\frac{3}{4}\right)$	$\left(\frac{1}{4};\frac{3}{4};\frac{3}{4}\right)$	$\left(\frac{1}{4};\frac{3}{4};\frac{3}{4}\right)$	$\left(0;0;\frac{1}{2}\right)$	$\left(0;0;\frac{1}{2}\right)$	$\left(0;0;\frac{1}{2}\right)$	$\left(0;0;\frac{1}{2}\right)$
		0.965	0.588	0.934	0.577	0.062	0.064	0.000	0.097
		0.965	0.588	0.934	0.577	0.062	0.175	0.000	0.084

	mag. mom.	0.965	0.588	0.934	0.577	0.062	0.175	0.000	0.084
		0.965	0.689	0.851	0.577	0.062	0.175	0.000	0.084

Table 1: Calculated magnetic moments (in μ_B / atom) and atomic positions (in reduced coordinates) for Ti atoms of all considered structures.

		Inverted				Regular			
		ideal	A2	B2	$D0_3$	ideal	A2	B2	$D0_3$
Mn	position	$\left(\frac{1}{2};\frac{1}{2};\frac{1}{2}\right)$	$\left(\frac{1}{2};\frac{1}{2};\frac{1}{2}\right)$	$\left(\frac{3}{4};\frac{1}{4};\frac{1}{4}\right)$	$(0;0;0)$	$\left(\frac{1}{4};\frac{1}{4};\frac{1}{4}\right)$	$\left(\frac{1}{4};\frac{1}{4};\frac{1}{4}\right)$	$\left(\frac{3}{4};\frac{1}{4};\frac{1}{4}\right)$	$\left(\frac{1}{4};\frac{1}{4};\frac{1}{4}\right)$
		$\left(\frac{1}{2};0;0\right)$	$\left(\frac{1}{2};0;0\right)$	$\left(\frac{1}{2};0;0\right)$	$\left(\frac{1}{2};0;0\right)$	$\left(\frac{3}{4};\frac{3}{4};\frac{1}{4}\right)$	$\left(\frac{3}{4};\frac{3}{4};\frac{1}{4}\right)$	$\left(\frac{3}{4};\frac{3}{4};\frac{1}{4}\right)$	$\left(\frac{3}{4};\frac{3}{4};\frac{1}{4}\right)$
		$\left(0;\frac{1}{2};0\right)$	$\left(0;\frac{1}{2};0\right)$	$\left(0;\frac{1}{2};0\right)$	$\left(0;\frac{1}{2};0\right)$	$\left(\frac{3}{4};\frac{1}{4};\frac{3}{4}\right)$	$\left(\frac{3}{4};\frac{1}{4};\frac{3}{4}\right)$	$\left(\frac{3}{4};\frac{1}{4};\frac{3}{4}\right)$	$\left(\frac{3}{4};\frac{1}{4};\frac{3}{4}\right)$
		$\left(0;0;\frac{1}{2}\right)$	$\left(0;0;\frac{1}{2}\right)$	$\left(0;0;\frac{1}{2}\right)$	$\left(0;0;\frac{1}{2}\right)$	$\left(\frac{1}{4};\frac{3}{4};\frac{3}{4}\right)$	$\left(\frac{1}{4};\frac{3}{4};\frac{3}{4}\right)$	$\left(\frac{1}{4};\frac{3}{4};\frac{3}{4}\right)$	$(0;0;0)$
	mag. mom.	-2.558	-1.424	-2.135	0.409	-0.220	-0.145	0.000	-0.429
		-2.558	-1.591	-2.347	-2.128	-0.220	-0.145	0.000	-0.429
		-2.557	-1.591	-2.347	-2.128	-0.220	-0.145	0.000	-0.429
		-2.558	-1.591	-2.347	-2.128	-0.220	0.142	0.001	0.041
Al	position	$\left(\frac{3}{4};\frac{1}{4};\frac{1}{4}\right)$	$(0;0;0)$	$\left(\frac{1}{2};\frac{1}{2};\frac{1}{2}\right)$	$\left(\frac{3}{4};\frac{1}{4};\frac{1}{4}\right)$	$\left(\frac{3}{4};\frac{1}{4};\frac{1}{4}\right)$	$(0;0;0)$	$\left(\frac{1}{4};\frac{1}{4};\frac{1}{4}\right)$	$\left(\frac{3}{4};\frac{1}{4};\frac{1}{4}\right)$
		$\left(\frac{1}{4};\frac{3}{4};\frac{1}{4}\right)$	$\left(\frac{1}{4};\frac{3}{4};\frac{1}{4}\right)$	$\left(\frac{1}{4};\frac{3}{4};\frac{1}{4}\right)$	$\left(\frac{1}{4};\frac{3}{4};\frac{1}{4}\right)$	$\left(\frac{1}{4};\frac{3}{4};\frac{1}{4}\right)$	$\left(\frac{1}{4};\frac{3}{4};\frac{1}{4}\right)$	$\left(\frac{1}{4};\frac{3}{4};\frac{1}{4}\right)$	$\left(\frac{1}{4};\frac{3}{4};\frac{1}{4}\right)$
		$\left(\frac{3}{4};\frac{3}{4};\frac{3}{4}\right)$	$\left(\frac{3}{4};\frac{3}{4};\frac{3}{4}\right)$	$\left(\frac{3}{4};\frac{3}{4};\frac{3}{4}\right)$	$\left(\frac{3}{4};\frac{3}{4};\frac{3}{4}\right)$	$\left(\frac{3}{4};\frac{3}{4};\frac{3}{4}\right)$	$\left(\frac{3}{4};\frac{3}{4};\frac{3}{4}\right)$	$\left(\frac{3}{4};\frac{3}{4};\frac{3}{4}\right)$	$\left(\frac{3}{4};\frac{3}{4};\frac{3}{4}\right)$
		$\left(\frac{1}{4};\frac{1}{4};\frac{3}{4}\right)$	$\left(\frac{1}{4};\frac{1}{4};\frac{3}{4}\right)$	$\left(\frac{1}{4};\frac{1}{4};\frac{3}{4}\right)$	$\left(\frac{1}{4};\frac{1}{4};\frac{3}{4}\right)$	$\left(\frac{1}{4};\frac{1}{4};\frac{3}{4}\right)$	$\left(\frac{1}{4};\frac{1}{4};\frac{3}{4}\right)$	$\left(\frac{1}{4};\frac{1}{4};\frac{3}{4}\right)$	$\left(\frac{1}{4};\frac{1}{4};\frac{3}{4}\right)$
	mag. mom.	0.037	0.091	0.008	0.022	0.004	0.002	0.000	0.017
		0.037	0.027	0.040	0.022	0.004	0.011	0.000	0.008
		0.037	0.027	0.040	0.022	0.004	0.011	0.000	0.008
		0.037	0.027	0.040	0.022	0.004	0.011	0.000	0.008

Table 2: Calculated magnetic moments (in μ_B / atom) and atomic positions (in reduced coordinates) for Mn and Al atoms of all considered structures.

Acknowledgments

This research is supported by the National Science Foundation (NSF) under Grant Numbers 2003828 and 2003856 via DMR and EPSCoR. This work used the Extreme Science and Engineering Discovery Environment (XSEDE), which is supported by National Science Foundation grant number ACI-1548562. This work used the XSEDE Regular Memory (Bridges 2) and Storage (Bridges 2 Ocean) at the Pittsburgh Supercomputing Center (PSC) through allocation TG-DMR180059, and the resources of the Center for Functional Nanomaterials, which is a U.S. DOE Office of Science Facility, and the Scientific Data and Computing Center, a component of the Computational Science Initiative, at Brookhaven National Laboratory (BNL) under Contract No. DE-SC0012704. Work at SUNY, Buffalo State was supported by the startup fund from SUNY Buffalo State and Undergraduate Research Office, Buffalo State.

References

1 R. A. de Groot, F. M. Mueller, P. G. van Engen, and K. H. J. Buschow, Phys. Rev. Lett. **50**, 2024 (1983).
2 I. Galanakis, P. H. Dederichs, and N. Papanikolaou, Phys. Rev. B **66**, 174429 (2002).
3 E. Şaşıoğlu, L. M. Sandratskii, P. Bruno, and I. Galanakis, Phys. Rev. B **72**, 184415 (2005).
4 S. Picozzi, A. Continenza, and A. J. Freeman, Phys. Rev. B **66**, 094421 (2002).
5 B. Balke, G. H. Fecher, J. Winterlik, and C. Felser, Appl. Phys. Lett. **90**, 152504 (2007).
6 J. Winterlik, S. Chadov, A. Gupta, V. Alijani, T. Gasi, K. Filsinger, B. Balke, G. H. Fecher, C. A. Jenkins, F. Casper, J. Kübler, G. Liu, L. Gao, S. S. P. Parkin, C. Felser, Adv. Mater. **24**, 6283 (2012).
7 I. Galanakis, Heusler Alloys (Springer Series in Materials Science, vol. 222) ed. C. Felser and A. Hirohata (Berlin: Springer, 2016).
8 I. Tutic, J. Herran, B. Staten, P. Gray, T. R. Paudel, A. Sokolov, E. Y. Tsymbal, and P. V. Lukashev, J. Phys.: Condens. Matter **29**, 075801 (2017).
9 J. Herran, R. Carlile, P. Kharel, and P. Lukashev, J. Phys.: Condens. Matter **31**, 495801 (2019).
10 R. Carlile, J. Herran, S. Poddar, E. Montgomery, P. Kharel, P. Shand and P. Lukashev, J. Phys.: Condens. Matter **33**, 105801 (2021).
11 X. L. Wang, Phys. Rev. Lett. **100**, 156404 (2008).
12 K. Özdoğan, E. Şaşıoğlu, and I. Galanakis, J. Appl. Phys. **113**, 193903 (2013).
13 H. Y. Jia, X. F. Dai, L. Y. Wang, R. Liu, X. T. Wang, P. P. Li, Y. T. Cui, and G. D. Liu, AIP Adv. **4**, 047113 (2014).
14 S. Ouardi, G. H. Fecher, and C. Felser, Phys. Rev. Lett. **110**, 100401 (2013).
15 P. Kharel, W. Zhang, R. Skomski, S. Valloppilly, Y. Huh, R. Fuglsby, S. Gilbert, and D. J. Sellmyer, J. Phys. D: Appl. Phys. **48**, 245002 (2015).

[16] I. M. Tsidilkovski, *Electron Spectrum of Gapless Semiconductors*, Spinger Series in Solid-State Sciences Vol. 116, edited by K. von Klitzing (Springer, New York, 1996).
[17] J. Herran, R. Dalal, P. Gray, P. Kharel, and P. Lukashev; J. Appl. Phys., **122**, 153904 (2017).
[18] B. Lv, P. Liu, Y. Miao, Z. Lian, M. Si, and C. Gao, Appl. Phys. Lett. **118**, 132408 (2021).
[19] S. Skaftouros, K. Özdoğan, E. Şaşıoğlu, and I. Galanakis, Appl. Phys. Lett. **102**, 022402 (2013).
[20] Q. Fang, X. Zhao, J. Zhang, and K. Xu, Thin Solid Films **558**, 241 (2014).
[21] W. Shi et al., Phys. Rev. B **97**, 060406(R) (2018).
[22] P. Lukashev, P. Kharel, S. Gilbert, B. Staten, N. Hurley, R. Fuglsby, Y. Huh, S. Valloppilly, W. Zhang, K. Yang, R. Skomski, and D. J. Sellmyer, Appl. Phys. Lett. **108**, 141901 (2016).
[23] J. Goraus and J. Czerniewski, J. Magn. Magn. Mater. **498**, 166106 (2020).
[24] W. Feng, X. Fu, C. Wan, Z. Yuan, X. Han, N. Quang, and S. Cho, Phys. Status Solidi RRL **9**, 641 (2015).
[25] P. Blöchl, Phys. Rev. B **50**, 17953 (1994).
[26] G. Kresse and D. Joubert, Phys. Rev. B **59**, 1758 (1999).
[27] J. P. Perdew, K. Burke, and M. Ernzerhof, Phys. Rev. Lett. **77**, 3865 (1996).
[28] M. Methfessel and A. T. Paxton, Phys. Rev. B **40**, 3616 (1989).
[29] MedeA-2.22, Materials Design, Inc., San Diego, CA, USA, 2017.
[30] J. Towns, T. Cockerill, M. Dahan, I. Foster, K. Gaither, A. Grimshaw, V. Hazlewood, S. Lathrop, D. Lifka, G. D. Peterson, R. Roskies, J. R. Scott, N. Wilkins-Diehr, "XSEDE: Accelerating Scientific Discovery", Computing in Science & Engineering, vol.**16**, no. 5, pp. 62-74, Sept.-Oct. 2014.
[31] K. Özdoğan and I. Galanakis, Phys. Rev. Materials **5**, 024409 (2021).
[32] J. P. Velev, P. A. Dowben, E. Y. Tsymbal, S. J. Jenkins, and A. N. Caruso, Surf. Sci. Rep. **63**, 400 (2008).
[33] X. Xu et al, Acta Materialia **176**, 33 (2019).
[34] J. Mooij, Phys. Status Solidi A **17**, 521 (1973).
[35] M. Jamer, B. Assaf, T. Devakul, and D. Heiman, Appl. Phys. Lett. **103**, 142403 (2013).
[36] P. Kharel, W. Zhang, R. Skomski, S. Valloppilly, Y. Huh, R. Fuglsby, S. Gilbert, and D. Sellmyer, J. Phys. D: Appl. Phys. **48**, 245002 (2015).
[37] W. Feng, X. Fu, C. Wan, Z. Yuan, X. Han, N. Quang, and S. Cho, Phys. Status Solidi RRL **9**, 641 (2015).